Effects of Hydrodynamic and Acoustic Pressure Fluctuations on Transmitted Sound in Wavenumber-Frequency Domain

Yasuhiko OKUTSU[1]; Naoki HAMAMOTO[1]

[1] Mitsubishi Motors Corporation, Japan

ABSTRACT

To control flow induced noise such as vehicle interior noise is very important for product development. In transmitted sound induced by flow field, a near acoustic field has to be considered. In this study, the wavenumber-frequency spectrum method was applied to the flow field around a square cylinder placed near a flat plate in order to examine pressure fluctuations in the near acoustic field. Since pressure fluctuations there contain both acoustic and hydrodynamic fluctuations, to deal with transmitted sound, both pressure fluctuations and structural bending waves have to be considered in this study. The flow field has been investigated by applying Computational Fluid Dynamics (CFD) based on the Lattice Boltzmann Method (LBM). The wavenumber-frequency spectrum was calculated by pressure fluctuations from CFD results. Thus, pressure field were investigated in wavenumber domain, and pressure fluctuations which contribute effectively to radiate the transmitted sound were extracted from all of them. As a result, it is concluded that the wavenumber-frequency spectrum method is useful to analyze flow induced noise such as vehicle interior noise.

Keywords: Flow, Noise, Transmission, Pressure I-INCE Classification of Subjects Number(s): 21.6

1. INTRODUCTION

Recently, the aerodynamic noise prediction technology for the environmental problem and getting comfort have become very important factors in the early stage of automobile, trains and airplanes development. Therefore, many researches on aerodynamic noise have been reported so far (1-3). Especially, because automobile aerodynamic noise is evaluated from inside of the cabin, the pressure fluctuations on a window glass or body panel which correspond to the noise generated in the near acoustic field must be considered. However, the near field contains both incompressible hydrodynamic pressure fluctuations and compressible acoustic ones.

The transmitted sound to the inside of a cabin is generated by oscillations of a window glass and a body surface. These oscillations are induced by hydrodynamic and acoustic pressure fluctuations. Therefore, it is significant to investigate pressure fluctuations in the near field. The wavenumber-frequency spectrum has been applied to analyze them recently. In this study, a square cylinder placed near a flat plate was provided as a consideration model. The flow field and sound field were calculated by a commercial CFD solver based on the Lattice Boltzmann Method (LBM) (4). The characteristic features of the flow structure and sound field in the near field obtained from the wavenumber-frequency spectrum (5-7) is described in what follows.

2. NOMENCLATURE

a	: Sound velocity [m/s]
$\vec{c}$	: Discrete velocity vector [m/s]
e	: Internal energy [J/s]
f	: Frequency [Hz]
f_i	: Particle distribution function
f_i^{eq}	: Local equilibrium distribution function

[1] yasuhiko.okutsu@mitsubishi-motors.com

i : Particle velocity direction
$\vec{k}$: Wavenumber vector [rad/m]
p : Pressure [Pa]
P : Power spectrum [dB]
$\vec{r}$: Distance vector [m]
S : Cross spectral density [dB/Hz]
t : Time [s]
U_c : Convective turbulent velocity [m/s]
v : Velocity [m/s]
$\vec{x}$: Position vector [m]
Φ : Wavenumber-frequency spectrum [dB/Hz]
ρ : Density [kg/m^3]
τ : Relaxation time parameter
ω : Angular frequency [Hz]

3. EXPERIMENTAL VERIFICATION

The test model was installed at the anechoic wind tunnel of Nagoya University (Fig. 1). The height (h) and the width of the square cylinder are 5mm; i.e. the aspect ratio is 1, and the span length is 40 h. The distance from the nozzle exit to the leading edge of the square cylinder is 10 h. The wind tunnel exit takes a square shape, the size of which is 20 h in the y direction $\times$ 20 h in the z direction, where the test flow velocity is 20m/s. The flat plate with a thickness of 0.1 h is made of aluminum. Two cases were examined by changing the distance d between the square cylinder and the flat plate; i.e. d =0 and 5 h. The far field noise level and the transmitted sound pressure level were measured by a 1/2 inch condenser microphone (B&K 4190).

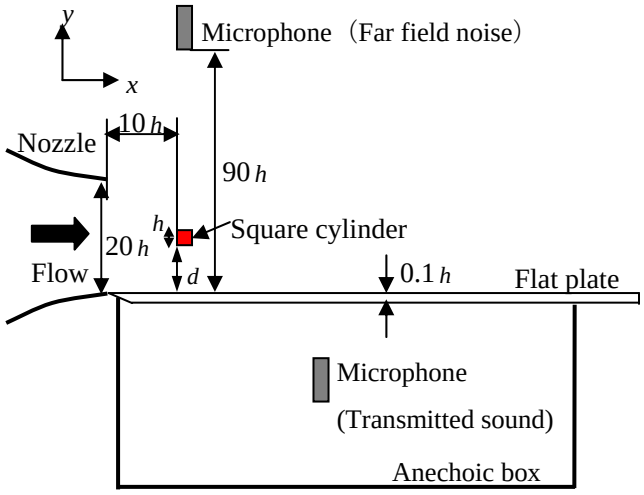

Figure 1 – Experimental apparatus (side view)

4. COMPUTATIONAL VERIFICATION

4.1 Numerical Scheme

The CFD commercial code PowerFLOW was used to compute the unsteady flow around the model. The code is based on the Lattice Boltzmann Method (LBM). Unlike conventional numerical methods for solving the Navier-Stokes equations, LBM deals with the "mesoscopic" level kinetic equation, based on the discrete Boltzmann equation for the particle distribution function, and quantities in the macroscopic fluid dynamics are obtained as a result of evolving the underlying particle distributions.

The lattice Boltzmann equation has the following form:

$$f_i(\vec{x}+\vec{c}_i\Delta t, t+\Delta t) - f_i(\vec{x},t) = -\frac{1}{\tau}\left[f_i(\vec{x},t) - f_i^{eq}(\vec{x},t)\right] \quad (1)$$

where f_i is the particle distribution function moving in the i th direction, based on a finite set of discrete velocity vectors. For simplicity and without loss of generality, the 3 dimensional 19 velocity (D3Q19) model was used in this study. $\vec{c}_i\Delta t$ and Δt are space and time increments, respectively. Regarding the collision term on the right hand side of Eq. (1), the simplest and most popular form, which is known as the Bhatnagar-Gross-Krook (BGK) form (8), is employed. τ is the single relaxation time parameter, and f_i^{eq} is the local equilibrium distribution function that depends on local hydrodynamic properties. The hydrodynamic quantities are obtained through moment summations as follows:

$$\begin{aligned} \rho(\vec{x},t) &= \sum_i f_i(\vec{x},t) \\ \rho\vec{v}(\vec{x},t) &= \sum_i \vec{c}_i f_i(\vec{x},t) \\ \frac{1}{2}\rho|\vec{v}(\vec{x},t)|^2 + \rho e &= \sum_i \frac{1}{2}|\vec{c}_i|^2 f_i(\vec{x},t) \end{aligned} \quad (2)$$

4.2 Numerical Conditions

A computational model, which is constructed with a square cylinder and a flat plate, is shown in Fig. 2. The span length of the square cylinder is enough long as compared to the width of the inlet. The dimensions of the calculation region are 1000 h in the x direction (the main flow direction), 950 h in the y direction (the normal direction to the plate) and 1000 h in the z direction (the spanwise direction). The inlet size is the same as the actual size of experimental apparatus, and the velocity of the uniform flow over the flat plate is 20m/s.

In terms of boundary conditions, at the outflow boundaries in the x-, y- and z-directions, the pressure was fixed and the velocity was extrapolated. The no-slip and adiabatic conditions were imposed on the surfaces of the square cylinder and the flat plate.

Regarding the grid employed here, 54 million grid points were used in the whole region, where the minimum grid size 0.5mm near the square cylinder. To obtain the significant data in the temporal frequency, the time step was set as 4.5×10^{-6}sec, and the total computation time is 1.0sec. The temporal and the spatial frequency response characteristics range from 20Hz to 5000Hz, considering the grid size around the model, the total calculation time, and the time of averaging.

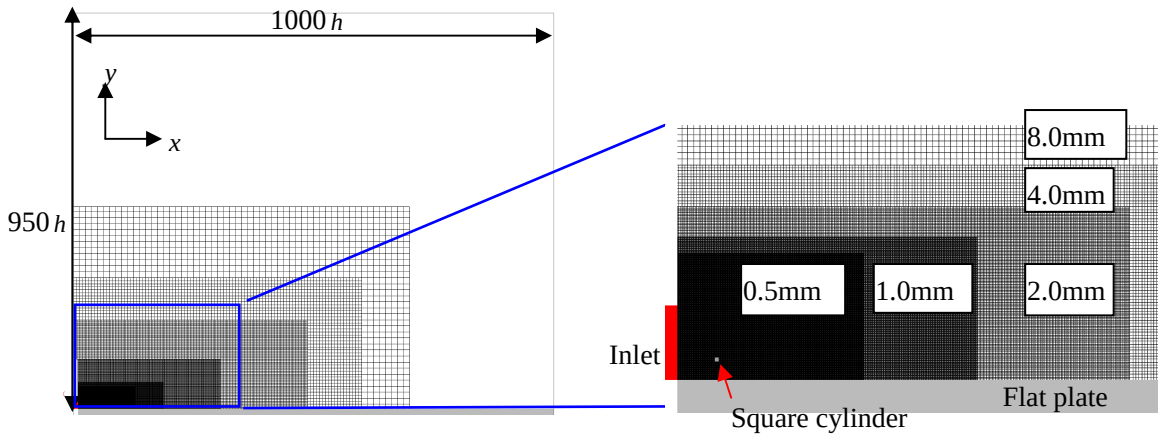

Figure 2 – Grids for computation

5. RESULTS AND DISCUSSION

5.1 Sound Field

The spectrums of far field noise level, which were measured in the experiment, are shown in Fig. 3. When $d = 5h$, there are two peaks: the 1st peak at 550Hz and the 2nd peak at 1100Hz, which caused by the Karman vortex street. In addition, in the high frequency range of 1000Hz or higher, the broad band noise level in the case of $d = 5h$ is larger than that in the case of $d = 0$. This suggests that the far filed noise level in the former is larger than in the latter.

On the other hand, with regard to the near filed, it is necessary to examine whether the same tendency can be observed in the near field. Contours of instantaneous pressure fluctuations in the near field are shown in Fig. 4, which was made from the time series data obtained by using a band pass filter. The acoustic pressure fluctuations, whose wavenumber is smaller than that of hydrodynamic ones, are seen in Fig. 4. In the case of $d = 5h$, the acoustic pressure fluctuations are predominant on the flat plate below the square cylinder. From these results, it is confirmed that there are both hydrodynamic and acoustic pressure fluctuations in the near field.

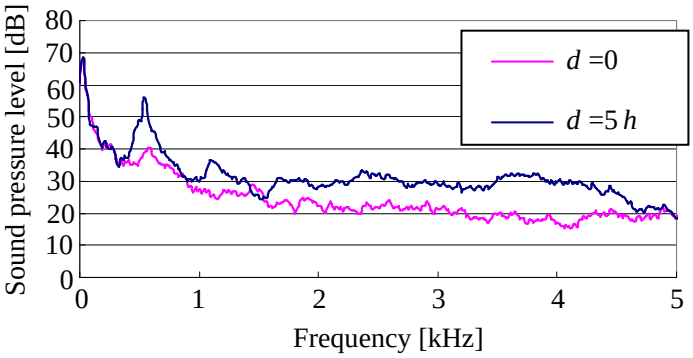

Figure 3 – Spectrum of far field noise level

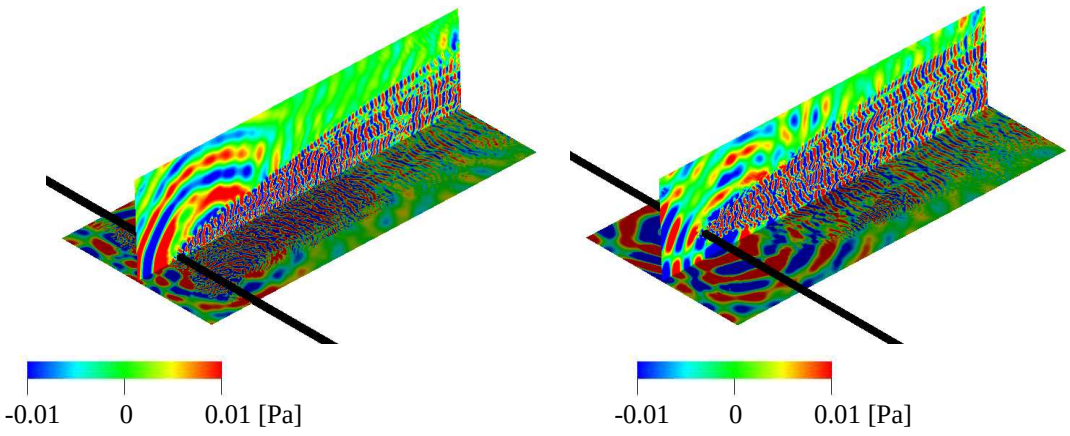

(a) $d = 0$ (b) $d = 5h$

Figure 4 – Instantaneous pressure fluctuations (2kHz-5kHz)

5.2 Flow Structure and Distribution of Surface Pressure Fluctuations

Two kinds of surface pressure fluctuations on the flat plate and the square cylinder are shown in decibel units in Fig. 5; the left side is in the frequency range of 250Hz-750Hz for low frequency pressure fluctuations, and the right side is in the range of 2000Hz-5000Hz for high frequency ones. In the case of $d = 0$, the pressure fluctuation level is high in the region behind the square cylinder. On the

other hand, in the case of $d = 5h$, since the interaction between the wake of the square cylinder and the flat plate is attenuated, the pressure fluctuation level becomes rather low on the flat plate. These interactions can be observed from contours of the z-directional vorticity component on the x-y plane (see Fig. 6). However, the pressure fluctuation level on the square cylinder is rather high in the range of 250Hz-750Hz, which is considered to be caused by the Karman vortex street with a frequency of about 550Hz.

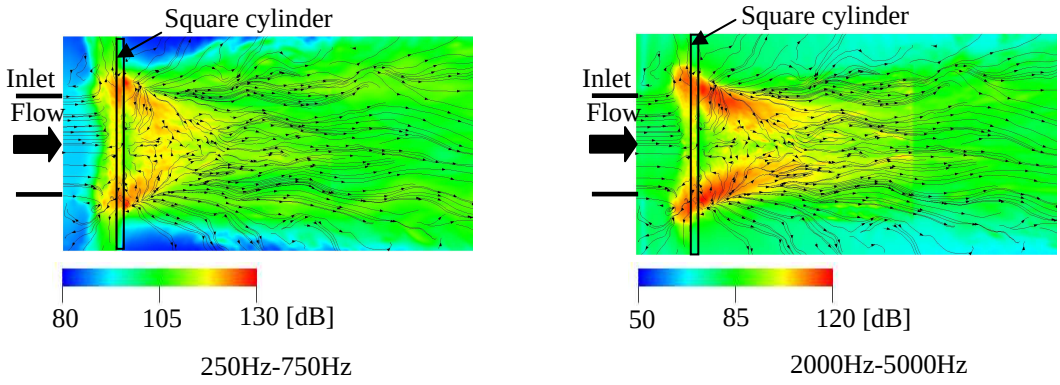

(a) $d = 0$

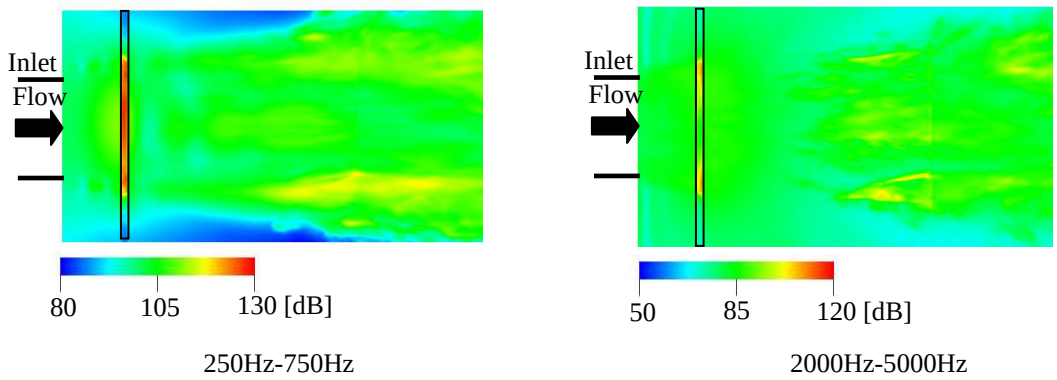

(b) $d = 5h$

Figure 5 – Contours of surface pressure fluctuation levels (Top view)

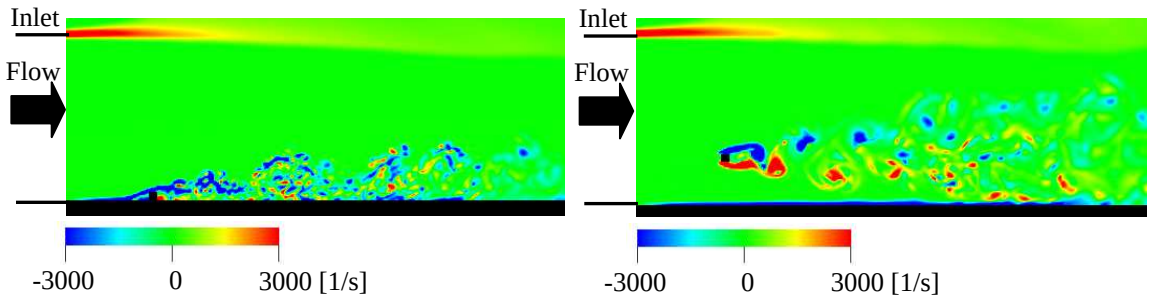

(a) $d = 0$ (b) $d = 5h$

Figure 6 – Contours of z-directional vorticity component on x-y plane

5.3 Wavenumber-Frequency Spectrum

To estimate the sound pressure level in the near field, it is necessary to take out only acoustic pressure fluctuations from the overall pressure fluctuations. However, it is difficult to separate hydrodynamic pressure fluctuations and acoustic ones in the time domain. Because the level of the

former is much higher than that of latter, the latter is buried by the former. Therefore, to deal with this issue in the wavenumber domain seems to be reasonable. The propagation speed of acoustic waves is exactly the same as the sound velocity, a, where $a \cong 340$m/s, the acoustic wavenumber, k_a, corresponds to the angular frequency, ω, as follows:

$$k_a = \omega / a \tag{3}$$

On the other hand, a turbulent flow contains various wavenumber components. Although the pressure fluctuations induced by airflow convection are not of a wave nature, in the wavenumber-frequency domain as a time-space correlation, the turbulent wavenumber k_c is determined by the convective turbulent velocity and the angular frequency as follows:

$$k_c = \omega / U_c \tag{4}$$

As the sound velocity is one order of magnitude larger than the convective turbulent velocity, it is possible to analyze separately hydrodynamic and acoustic pressure fluctuations by wavenumber vectors.

The Fourier transform from the time domain to the frequency domain is written by

$$P(\vec{r}, \omega) = \frac{1}{2\pi} \int_{-\infty}^{\infty} p(\vec{r}, t) e^{-j\omega t} dt \tag{5}$$

The cross spectral density is defined as follows:

$$S_{P_i P_j}(\vec{x}_i, \vec{r}, \omega) = \frac{P(\vec{x}_i, \omega) P^*(\vec{x}_j = \vec{x}_i + \vec{r}, \omega)}{\Delta f} \tag{6}$$

where Δf means frequency band width and $*$ means conjugate.

The spatial average of Eq. (6) based on the assumption of ergodicity leads to the following form:

$$S_{P_i P_j}(\vec{r}, \omega) = \frac{E\left[P(\vec{x}_i, \omega) P^*(\vec{x}_j = \vec{x}_i + \vec{r}, \omega)\right]}{\Delta f} \tag{7}$$

where $E[\cdot]$ stands for an expected value.

Similarly, the Fourier transform from the spatial domain to the wavenumber domain is written by

$$P(\vec{k}, t) = \frac{1}{2\pi} \int_{-\infty}^{\infty} p(\vec{x}, t) e^{-j\vec{k}\vec{x}} d\vec{x} \tag{8}$$

The cross spectral density is a function of frequency and wavenumber, and is generally referred to as the wavenumber-frequency spectrum. This can be obtained by the spatial Fourier transform of $S_{P_i P_j}(\vec{r}, \omega)$. That is to say, the wavenumber-frequency spectrum is the time-space correlation function of the pressure field. Therefore, the one-dimensional wavenumber-frequency spectrum is expressed by the following expression:

$$\Phi(\vec{k}, \omega) = \frac{1}{2\pi} \int_{-\infty}^{\infty} S_{P_i P_j}(\vec{r}, \omega) e^{-j\vec{k}\vec{r}} d\vec{r} \tag{9}$$

The domain of integration in the x, y and z directions to calculate the one dimensional wavenumber-frequency spectrum is shown in Fig. 7, and results are indicated in Figs. 8 and 9. The horizontal axis means the wavenumber $k = 2\pi/\omega$[rad/m], the longitudinal axis the frequency f [kHz] and the color scale is the magnitude of pressure fluctuations.

Acoustic wavenumber lines in results of the wavenumber-frequency spectrum (see Figs. 8 and 9) are defined by Eq. (3). Wavenumber vectors on the acoustic wavenumber lines are acoustic components propagating along each line for analysis (6). Diffuse acoustic components are included inside the region enclosed by the acoustic wavenumber lines (7). The turbulent components that have larger wavenumbers than the acoustic components exist in the region outside the acoustic wavenumber lines (6).

The acoustic pressure fluctuations are predominant in the 3kHz or higher frequency region (see Figs. 8 and 9). In addition, since convection ridges are shown in wavenumber-frequency spectrum results, the convective velocity can be estimated by Eq. (4). For example, in the case of d =0, the convective velocity U_c is about 11m/s along the x1 line, and the velocity is 20m/s in the case of d =5 h.

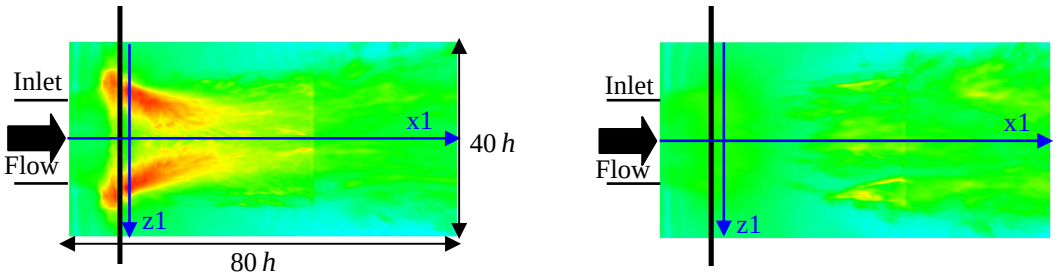

(a) d =0 (b) d =5 h

Figure 7 – Analysis lines of the one dimensional wavenumber-frequency spectrum

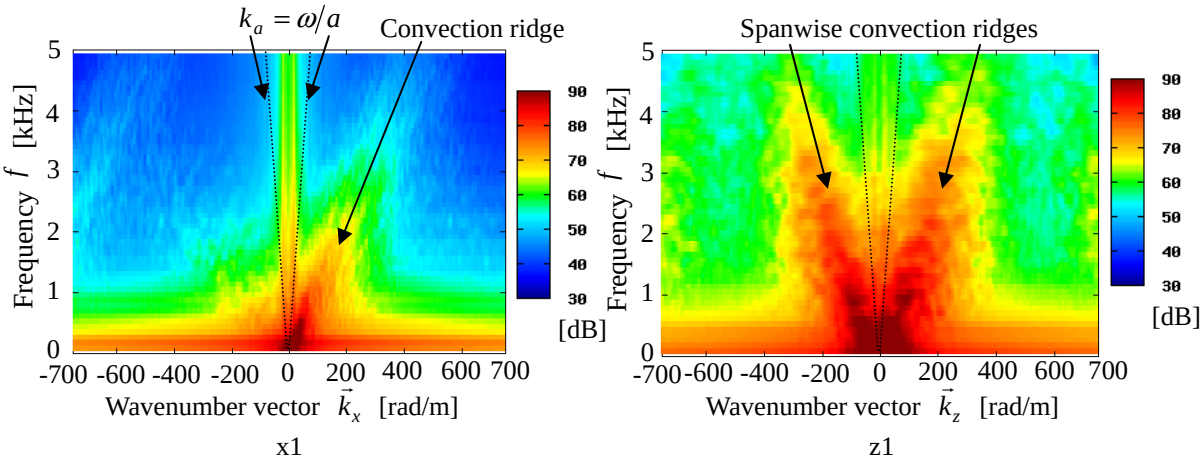

Figure 8 – Wavenumber-frequency spectrums (d =0)

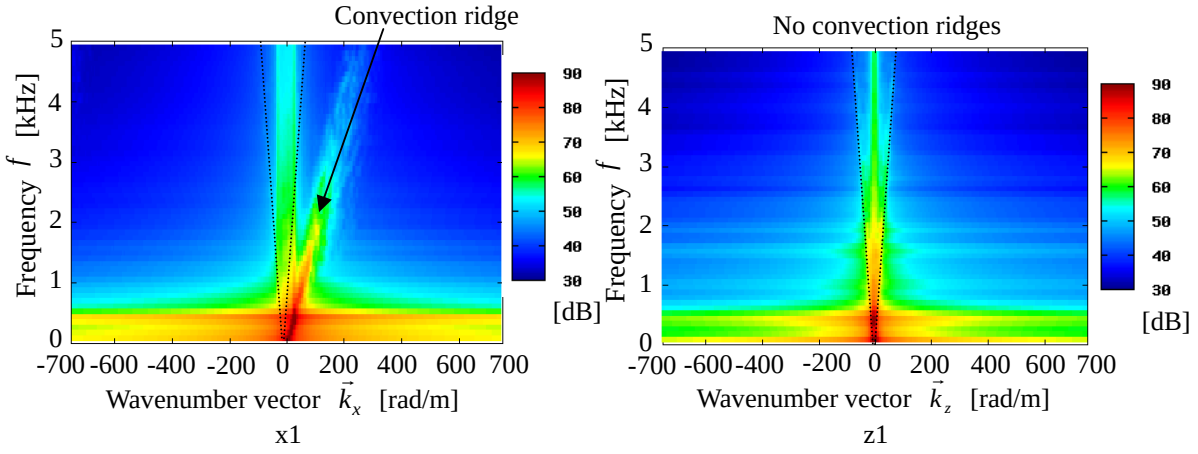

Figure 9 – Wavenumber-frequency spectrums (d =5 h)

To compare quantitatively the acoustic and turbulent flow fluctuation level on the flat plate surface between the case of d =0 and d =5 h, the magnitude of acoustic and turbulent flow pressure fluctuations were calculated by integrating the wavenumber-frequency spectrum as follows:

Acoustic fluctuation:

$$\int \Phi(\vec{k},\omega)d\vec{k} \qquad |\vec{k}| \le k_a \tag{10}$$

Turbulent flow fluctuation:

$$\int \Phi(\vec{k},\omega)d\vec{k} \qquad |\vec{k}| > k_a \tag{11}$$

These results are shown in Fig.10. As mentioned earlier, the sound pressure level at a frequency of 1kHz or higher in the case of $d=5h$ is larger than that in the case of $d=0$ in the far field (see Fig. 3). On the other hand, in the near field, the acoustic fluctuation level in the case of $d=0$ is higher than that in the case of $d=5h$ in the high frequency region. This tendency is observed in the measurement of transmitted sound on the opposite side of the flat plate in an anechoic box (Fig.11). The wavenumber-frequency spectrum method is useful for estimating of hydrodynamic pressure fluctuations and acoustic ones in the near filed separately. Therefore this method should be used effectively for estimating the transmitted sound hereafter. Specifically, since pressure fluctuations in acoustic wavenumber components (Eq. (10)) are input power for effectively radiated sound from oscillations of a flat plate, they are important for estimation of transmitted sound as described below.

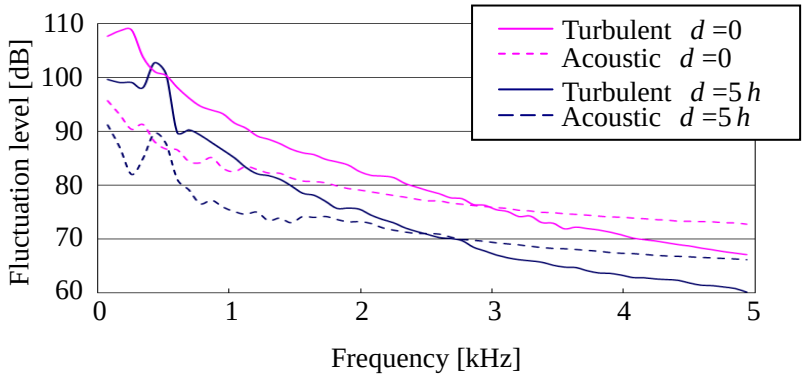

Figure 10 – Acoustic and turbulent fluctuation levels along the x-direction

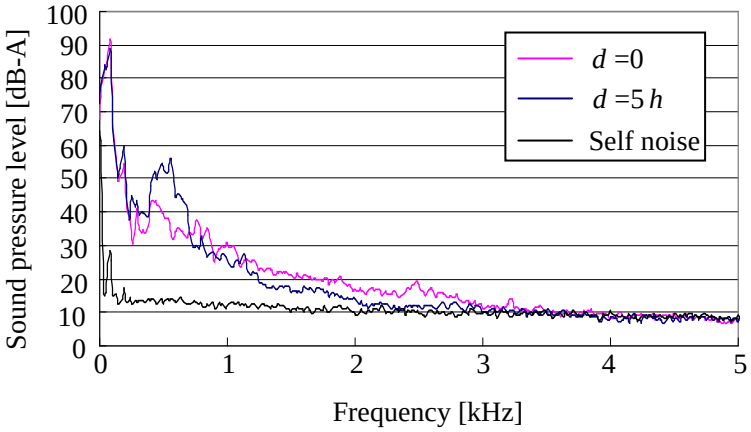

Figure 11 – Measured transmitted sound level in the anechoic box

5.4 Transmitted Sound Radiated from Flat Plate

To discuss about the transmitted sound radiated from the flat plate, it needs to consider about bending waves of a flat plate. For vehicle transmission noise, thickness of outer body panels and window glasses are too thin to consider longitudinal wave in the panels or glasses. Therefore, transverse waves are important. In actual, coincidence effects and eigenvalues of bending waves which are decided by constraint conditions are needed to consider. However, in this study, as a first step, bending waves in an infinite flat plate and transmission noise radiated from it are considered in the wavenumber space. Considering the acoustic wavenumber circle (9) and the radiation sphere help us to understand the phenomenon of sound radiation from bending waves. Wavenumbers of the

aluminum flat plate's bending waves have k_x and k_z components. So, the flat plate's wavenumber is written by

$$k_p = \sqrt{{k_x}^2 + {k_z}^2} \tag{12}$$

There are two situations about these k_x and k_z values. One is they are in acoustic wavenumber circle (see Fig. 12(a)). The other is either or both of k_x and k_z is outside the circle (see Fig. 12(b)). In the former case i.e. $k_a > k_p$, radiation sound's wavenumber k_y is written by

$$k_y = \sqrt{k^2 - ({k_x}^2 + {k_z}^2)} = \sqrt{k^2 - {k_p}^2} \tag{13}$$

Since k_y is real number, by substituting k_y into $e^{j(\omega t - k_y y)}$, it is found that a wave which fluctuates and propagates in time-space domain radiate from the flat plate's bending waves. The other hand, in the case of the latter situation i.e. $k_a < k_p$, k_y is written by

$$k_y = \sqrt{{k_a}^2 - ({k_x}^2 + {k_z}^2)} = \sqrt{-({k_p}^2 - {k_a}^2)} = j\sqrt{{k_p}^2 - {k_a}^2} \tag{14}$$

Thus k_y is imaginary number, by substituting k_y into $e^{j(\omega t - k_y y)}$, it is found that $e^{j(\omega t - k_y y)} = e^{j\omega t + \sqrt{{k_p}^2 - {k_a}^2} y}$. Therefore, this wave fluctuates in time, but do not propagate in space. Such wave is called evanescent wave.

From this theoretical analysis, acoustic wavenumber components are important for considering transmission noise, and it seems that reducing pressure fluctuations in acoustic wavenumber components is useful for effective reduction of the transmitted sound level. Therefore, to extract acoustic wavenumber components of pressure fluctuations in the near acoustic field, the wavenumber-frequency spectrum method is useful.

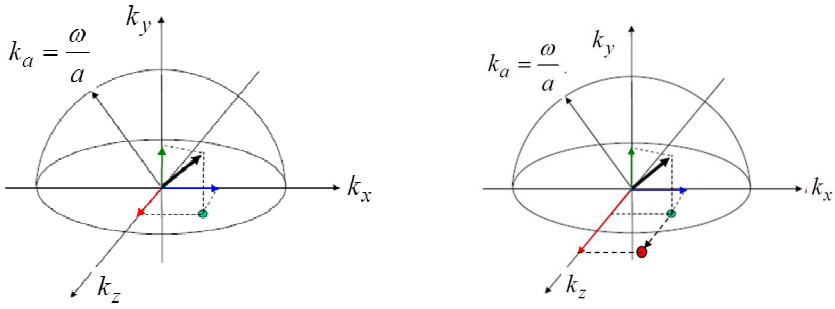

(a) $k_a > k_p$ (b) $k_a < k_p$

Figure 12 – Acoustic wavenumber circle and radiation sphere

6. CONCLUSIONS

In this study, pressure fluctuations in the near acoustic field were investigated by the wavenumber-frequency spectrum method. The following conclusions are derived from results obtained here.

(1) The far field noise level in the case of d =5 h is larger than that in the case of d =0 in the frequency range of 500Hz or higher. However, the transmission noise level in the anechoic box shows the opposite tendency; i.e., the noise level in the case of d =5 h is lower than that in the case of d =0 in the frequency range of the 1000Hz or higher.

(2) Acoustic and turbulent flow pressure fluctuation levels as well as convective velocities in the near acoustic field can be estimated by the wavenumber-frequency spectrum method employed

here.

(3) It was found that acoustic pressure fluctuations are predominant compared with turbulent flow ones at higher frequencies in the near acoustic field.

(4) To reduce transmission noise effectively, reduction of pressure fluctuations in acoustic wavenumber components is useful. As the next step, to construct prediction method for transmission noise, coincidence effects and eigenvalues of bending waves which are decided by constraint conditions are needed to consider.

REFERENCES

1. Mejia P, Park J, and Mongeau L. Surface Pressure Fluctuations in Separated-Reattached Flows Behind Notched Spoilers. SAE Paper; 2007-01-2339. 2007.
2. Kato C, Murata O, Kokubo A, Ichinose K, Kijima T, Horinouchi N, and Iida A. Measurements of Aeroacoustic Noise and Pressure Fluctuation Generated by a Door-Mirror Model Placed on a Flat Plate. Journal of Environment Engineering; Vol.2, No.2, 2007. pp. 278-292.
3. Takaishi T, Sagawa A, and Kato C. Numerical Analysis of Aerodynamic Noise Emitted from a Pantograph Based on Non-compact Green's Function. Journal of Environment Engineering; Vol.5, No.1, 2010. pp. 84-96.
4. Tsutahara M, Takada N, and Kataoka T. Lattice Gas Cellular Automata / Lattice Boltzmann Method. corona publishing 1999. p. 56-84. (in Japanese)
5. Howe M. S. The Turbulent Boundary-Layer Rough-Wall Pressure Spectrum at Acoustic and Subconvective Wavenumbers. Proceedings of the Royal Society of London A; Vol.415, 1998. pp. 141-1616.
6. Howe M. S. Acoustics of Fluid-Structure Interactions. Cambridge University Press 1998. p. 204-210.
7. Arguillat B, Ricot D, Bailly C, and Robert G. Measured wavenumber: Frequency spectrum associated with acoustic and aerodynamic wall pressure fluctuations. Journal of the Acoustical Society of America; Vol.128, No.4, 2010. pp.1647-1655.
8. Bhatnagar P, Gross E, and Krook M. A Model for Collision Processes in Gases. I. Small Amplitude Processes in Charged and Neutral One-Component Systems. Physical. Review; vol.94, 1954. pp.511-525.
9. Williams, E.G. Fourier Acoustics Sound Radiation and Nearfield Acoustical Holography. Springer-Verlag Tokyo 2005. p.23-56. (in Japanese)